Journal of Power Sources 187 (2009) 575–580

Contents lists available at ScienceDirect

Journal of Power Sources

journal homepage: www.elsevier.com/locate/jpowsour

Macroporous poly(vinylidene fluoride) membrane as a separator for lithium-ion batteries with high charge rate capacity

D. Djian[a], F. Alloin[b,*], S. Martinet[a], H. Lignier[a]

[a] CEA-LITEN, 17 rue des martyrs, 38054 Grenoble Cedex 9, France
[b] Laboratoire d'Electrochimie et de Physico-chimie des Matériaux et des Interfaces – LEPMI, UMR 5631 CNRS-INPG-UJF, BP 75, 38402 Saint-Martin-d'Hères Cedex, France

ARTICLE INFO

Article history:
Received 16 May 2008
Received in revised form 26 October 2008
Accepted 1 November 2008
Available online 18 November 2008

Keywords:
$Li_4Ti_5O_{12}$
PVdF
Macroporous membrane
Lithium-ion battery
High charge rate

ABSTRACT

The performance of PVdF macroporous separators used in lithium battery at high charge rates was evaluated using $Li_4Ti_5O_{12}$ and $LiMn_2O_4$ as negative and positive electrodes respectively. The effects of the non-solvent used, the PVdF concentration in the good solvent and the thickness of the swelled membrane on membrane porosity and on the conductivity of the separator + liquid electrolyte were evaluated. The conductivity decrease, induced by the porous separator introduction and separator thickness influence notably battery performance for high charge rate.

1. Introduction

Lithium-ion batteries are currently used in a range of portable electronic devices. To expand the application field of the lithium-ion battery, an improvement in high charge rate capability is needed. The rate capability limitation of lithium-ion batteries is a result of several factors, namely the solid state diffusion of lithium ions [1], the charge transfer kinetics reaction, the concentration gradient in the electrolyte (bulk electrolyte, porous electrode), the ionic conductivity in the electrolyte or in the electrode or the electrode electronic conductivity. All these processes could be limiting processes [2,3]. Furthermore, the limiting processes depend on the charge and discharge rates during the cycling test. Solid state diffusion of lithium in active materials has been improved by using nanostructured lithium intercalated compounds [4] and through well-adapted electrode design [3]. The influence of the morphology of the commercial separator, i.e. polyolefin, on high charge rate performance has been evaluated [5]. Most of the commercial porous separators induced a sharp decrease in the conductivity of the liquid electrolyte. The MacMullin number multiplied by the separator thickness seems to be a relevant indicator for defining a good electrolyte adapted to high charge rates [5].

Poly(vinylidene fluoride), PVdF, is a commercially available fluoropolymer. The advantage of PVdF macroporous separators compared with polyolefin separators is their good ability to be wetted by organic solvents and their ability to enable good electrode/electrolyte contact. PVdF membranes were intensively studied as electrolyte for lithium battery. Appetecchi et al. [6–8] studied the use of PVdF copolymers as electrolyte for lithium battery; good performance in term of conductivity was obtained.

Tarascon et al. [9] using an innovative technology based on lamination of fluorinated copolymers, manufactured "plastic rechargeable Li-ion batteries", claimed for a plastic $LiMn_2O_4$/graphite battery, specific and volumetric energies of respectively 110 Wh kg^{-1} and 280 Wh l^{-1} and a lifespan > 2000 cycles at 25 °C (rate: 1*C*). Du Pasquier et al. [10] reported the performances of $LiMn_2O_4$/graphite batteries of 35 and 115 mAh, based on PVdF-HFP macroporous separator. The capacity retention of the 35 mAh at a *C*/2 rate and at room temperature ranges between 80% and 70% after 500 cycles.

Macroporous PVdF membranes are generally prepared by an immersion–precipitation technique, in which a PVdF solution-casting film is immersed in a precipitation bath. For a crystalline polymer such as PVdF, the precipitation process may be governed by either crystallization or liquid–liquid demixing, depending on the harshness of the coagulation bath [11]. The preparation parameters can be adjusted to yield a wide variety of membrane morphologies.

Graphite has been largely used as an anode in lithium-ion batteries. While graphite can be used for high discharge rates, it is

* Corresponding author. Tel.: +33 4 76 82 65 61; fax: +33 4 76 82 65 77.
E-mail address: Fannie.alloin@enseeg.inpg.fr (F. Alloin).

0378-7753/$ – see front matter © 2008 Elsevier B.V. All rights reserved.
doi:10.1016/j.jpowsour.2008.11.027

not recommended for high charge rates. Indeed, at high charge rates, metallic lithium deposits have been observed on the graphite surface, leading to dendrite formation. The dendrites can grow rapidly through the macroporous electrolyte, and induce short circuits. $Li_4Ti_5O_{12}$ is a negative electrode material that can be used as an alternative to graphite for fast charge Li-ion systems [12]. Furthermore, $Li_4Ti_5O_{12}$ electrode has a potential equal to 1.5 V vs Li/Li^+, potential where the electrolyte is thermodynamic stable.

This paper deals with the evaluation the electrochemical behaviour of lithium batteries using a macroporous PVdF separator and $Li_4Ti_5O_{12}$ and $LiMn_2O_4$ as negative and positive electrodes respectively during high charge rate cycling tests. Indeed at classical charge rates, charge rates between *C*/10 and 2*C*, the morphology of macroporous membrane has a small impact on the capacity values. The impact of the morphology of macroporous PVdF separators i.e. porosity amount, thickness on the electrochemical behaviour at high charge rate cycling tests of lithium batteries equipped with such separators were evaluated.

2. Experimental details

2.1. Preparation of the PVdF macroporous membrane

The thick macroporous PVdF membranes were prepared as follows: PVdF Solef® 6020 (Solvay) was dissolved in *N*-methyl-2-pyrollidone (NMP) at 60 °C in a hermetically sealed vessel. Indeed due to the high crystallinity content of PVdF homopolymer, its dissolution was only possible at high temperature. The solution was then cast using a coating table in a glove box, which enabled the film thickness to be controlled. The solution was then put immediately into a precipitation bath for a few minutes. The presence of a large amount of non-solvent involves the precipitation of the polymer which induces the formation of a porous structure. The obtained membrane was dried at 55 °C overnight, then at 120 °C in vacuum for 48 h and stored in glove box.

2.2. Liquid electrolyte

The experimental liquid electrolyte was LP30® manufactured by Merck. The electrolyte used was a molar solution of $LiPF_6$ in a 1/1 (in weight) mixture of ethylene carbonate (EC) and dimethyl carbonate (DMC). The electrolyte was stored in a glove box under dry argon. The macroporous membranes were swelled in liquid electrolyte for several hours, thus the membranes were placed rapidly in the conductivity cell, and a small amount of liquid electrolyte was added in order to fill the porosity.

2.3. Electrode

The positive electrode consisting of a manganese spinel ($LiMn_2O_4$) was a commercial grade electrode purchased from Erachem. The insertion potential of this material is 4.1 V vs Li/Li^+ and its specific capacity is 120 mAh g^{-1} [13]. The intercalated material for the negative electrode was a home-made lithiated titanium oxide $Li_4Ti_5O_{12}$ with a lithium insertion potential of 1.55 V vs Li/Li^+ and a specific capacity equal to 160 mAh g^{-1} [14]. The composite electrodes were prepared by blending $Li_4Ti_5O_{12}$ and $LiMn_2O_4$ powder with 6% acetylene black, 6% fibrous carbon and 6% poly(vinylidene fluoride) (Solef® 1015, Solvay). The current collector was 20 μm thick aluminium foil. The thicknesses of the coating of the electrodes were 14 and 80 μm for the negative and positive electrodes respectively. The area capacity densities were 2 (±0.1) mAh cm^{-2} and 0.4 (±0.05) mAh cm^{-2} for the positive and negative electrodes respectively. The area capacity density of each cell was determined with good accuracy; measurement precision was about 3%. Electric percolation, porosity volume and adhesion of the electrodes to the aluminium foil were achieved by compression. The resulting electrodes were dried under vacuum at 80 °C for 48 h.

2.4. Nonlinear mechanical properties

Nonlinear mechanical properties were studied by tensile tests performed with an Instron 4465 Machine equipped with a thermo regulated chamber. The sample section was 2 mm × 35 mm. Experiments were carried out at 20 °C. The stretching was performed at a constant crosshead speed of 1 mm min^{-1}.

2.5. Ionic conductivity measurements

Conductivity measurements were carried out in CR2032 coin cells assembled and sealed in a glove box under dry argon (<2 ppm H_2O). The metallic components were dried under vacuum at 120 °C for 48 h. Blocking electrodes were made from 16 mm diameter stainless steel. The cell constant was determined with good accuracy using KCl solution in Viledon® separator and was found to be in accordance with the electrode area and the thickness of the sample. This cell constant was used to determine the real area of the electrode; the thickness was determined by several measurements on the macroporous membranes. All measurements were performed 3 times, with precision of about 15%, using impedance spectroscopy over the frequency range 1 Hz to 1.3 MHz with ±10 mV amplitude around the OCV, using a Solartron SI 1260 analyser equipped with a Solartron SI 1287 interface. One impedance spectrum limited to the high frequencies is given in Fig. 1.

2.6. Cycling test

The cycling tests were performed on an Arbin® multichannel system, using CR2032 coin cells first sealed in a glove box under dry argon. A stainless steel disc and a spring ensured the cohesion of the system.

The cycling tests were performed in galvanostatic mode. The cut-off limits were related to the voltage of the battery: 2.9 V in

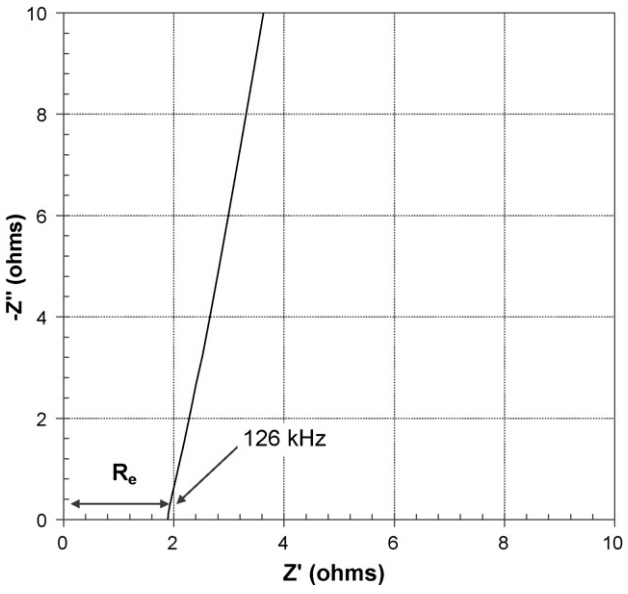

Fig. 1. Impedance spectrum performed on macroporous PVdF membrane swelled by the liquid electrolyte between to stainless steel electrodes.

charge, 1 and 1.5 V for high or low discharge rates respectively. These voltage limits were used to prevent over-discharge and over-charge. The charge/discharge yield was close to 100% even at high charge rates. The experiments were performed several times for each battery and each charge rate.

3. Results and discussion

3.1. Macroporous structure of PVdF

PVdF membranes were prepared by an immersion–precipitation method. The precipitation baths consisted of water, ethanol or pentanol. PVdF may be precipitated from a poor solvent bath by either liquid–liquid segregation or crystallization to produce several membrane morphologies. According to the Flory–Huggins description of polymer solutions, the size and location of the demixing gap depends on the molar volumes of the components, the polymer–solvent interaction parameter, the polymer–non-solvent interaction parameter and the solvent–non-solvent interaction parameter. The effect of the polymer–solvent interaction on the structure and properties of the membrane has been studied [15,16]. It is generally observed that the lower these interactions, the higher the rate of polymer precipitation, with the formation of finger-like structures. The polymer–solvent and polymer–non-solvent interaction parameters can be characterized with the Hansen solubility parameters. The more similar the polymer and the solvent structure are, the closer the polymer and solvent parameters are. To characterize the solvent/polymer interaction, the critical solubility radius can be used [17]. The critical solubility radiuses are 16.8, 5.6 and 4.8 $(J\,cm^{-3})^{1/2}$ for respectively PVdF/water, PVdF/ethanol and PVdF/pentanol. The greater the critical solubility radius is, the lower the solubility is. Boudin et al. [18] determined that propylene carbonate was the worst latent solvent, with a solubility radius equal to 4.78 $(J\,cm^{-3})^{1/2}$. Thus pentanol is very close to the PVdF solubility sphere and water is a very poor solvent for PVdF. The solvent–non-solvent mutual diffusivity also has a big impact on PVdF macroporous membrane structure [15].

The immersion of PVdF/NMP solution in a water bath induces a very rapid precipitation process with the formation of an asymmetric porous structure i.e. the presence of a skin at the membrane surface and some macrovoids in the bulk, in accordance with the observations made by Lin et al. and Bottino et al. [11,15]. The liquid–liquid phase demixing process dominates the precipitation process [11]. This effect may be related to the high critical solubility radius of PVdF/water. The presence of a skin on the porous membrane induces an internal resistance increase due to the poorly conducting surface layer, which is fatal for high charge rate performance of batteries.

In order to obtain a soft coagulation bath, ethanol and pentanol were used as non-solvents. The precipitation process slows down and the formed membrane demonstrates a mixed morphology featuring both liquid–liquid demixing and a crystallization process, in accordance with previous studies [11,19]. The PVdF morphologies obtained with these two solvents are very similar, the porous structure is homogeneous and no skin is observed (Fig. 2).

Using ethanol and pentanol as non-solvents, the effects of the non-solvent used, the PVdF concentration in NMP and the thickness of the swelled membrane on the conductivity of the separator + liquid electrolyte and membrane porosity were evaluated.

Membrane porosity was determined using the weight and size of the sample in relation to the density of the PVdF. The mercury porosity technique was used to determine the pore sizes. The PVdF porous membranes obtained in ethanol or pentanol present a broad distribution of pore sizes, with a median diameter of 10 μm. No pore passes through the membrane, creating a tortuosity and limiting the transfer of electrode particles between the anode and the cathode. Porosity depends on both the PVdF concentration in NMP and the nature of the non-solvent. The experiments performed with the same experimental parameters show good reproducibility (Table 1), the reproducibility was confirmed by two series of membranes (PVdF-1 and PVdF-2, PVdF-3 and PVdF-4). The membranes

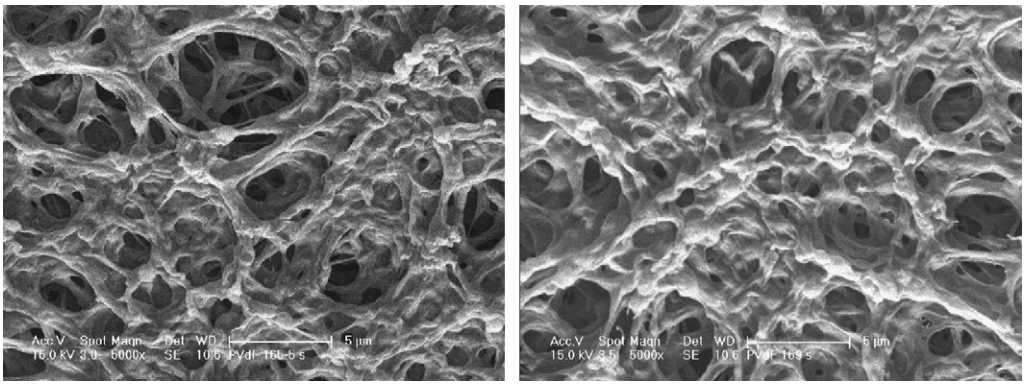

Fig. 2. Scanning electron microscopy of the PVdF macroporous membrane surface (a) ethanol precipitation bath (b) pentanol precipitation bath (×5000).

Table 1
Thickness and porosity of PVdF macroporous separators. Influence of process parameters on the macroporous membrane characteristics.

Sample	Swelled membrane thickness (μm)	PVdF concentration in NMP (%)	Non-solvent	Thickness (μm)	Porosity (%)
PVdF-1	200	17	Ethanol	42 ± 2	66 ± 3
PVdF-2	200	17	Ethanol	46 ± 2	68 ± 2
PVdF-3	200	13	Ethanol	44 ± 2	77 ± 3
PVdF-4	200	13	Ethanol	43 ± 2	76 ± 3
PVdF-5	400	17	Ethanol	70 ± 2	58 ± 2
PVdF-6	200	17	Pentanol	37 ± 2	58 ± 2
PVdF-7	200	13	Pentanol	35 ± 2	66 ± 3

Table 2
Mechanical properties of PVdF macroporous membrane and Celgard® 2500.

	Thickness (μm)	Porosity (%)	Breaking nominal stress (MPa)	Breaking nominal strain (%)
Celgard® 2500	23 ± 2	47 ± 8	60 ± 10	18 ± 0.6
PVdF	44 ± 5	77 ± 1	5 ± 1	34 ± 0.5

performed with the same experimental conditions i.e. concentration, thickness, non-solvent, present the same thickness and porosity amount (Table 1). The increase in PVdF concentration induces a decrease in the amount of porosity. The use of pentanol as a non-solvent induces a decrease in the porosity of the PVdF membrane in comparison with the membrane prepared in the ethanol coagulation bath (Table 1). The membrane obtained in the pentanol coagulation bath (thickness 200 μm, concentration 13%) presents a porosity of 66% whereas the porosity of the membrane obtained in the ethanol coagulation bath (thickness 200 μm, concentration 13%) is equal to 76%. The increase in thickness of the swelled membrane has no effect on the porosity amount; the only effect is an increase in the thickness of the dry membrane obtained. The modification of the polymer concentration in solution and the non-solvent use permit to performed macroporous membranes with similar porosity structure (pore size and shape) but with different porosity amount.

Table 2 gives the mechanical properties of PVdF macroporous membrane in comparison of those obtained with porous Celgard® 2500 membrane. The PVdF macroporous membrane presents lower mechanical properties than Celgard® 2500, with a breaking nominal stress ten times lower. However, the macroporous PVdF membrane can be prepared directly on the electrode, thus the mechanical properties are ensure by the electrode.

The thermal degradation of PVdF starts from 390 °C, producing HF by-product [20]. It is in addition very resistant to the majority of inorganic acids, halogens and oxidants. DSC shows that the macroporous membrane swollen by the electrolyte starts to melt near 80 °C. For the macroporous membrane free of solvent, the melting point is much higher and begins at 140 °C. The plugging up of the membrane porosity, which occurs at 80 °C can perform a beneficial shut down effect as in polyolefin separator.

3.2. Conductivity characterization

Porous separators prevent shorts but they decrease the ionic conductivity of liquid electrolytes. The conductivity measurements of macroporous membrane swelled by the electrolyte were performed using LP30® liquid electrolyte, EC/DMC (50/50 in volume) 1 M $LiPF_6$, (σ_0 = 9.8 mS cm^{-1}). The results of conductivity are shown in Table 3. The shapes of the conductivity curves for the liquid electrolyte alone and the same one filling the macroporous PVdF are identical at room temperature. As the pores were interconnected, the impedance spectra present no signature associated to the conductivity of the dense membrane swelled by the electrolyte (Fig. 1). The effective way for the conduction is defined only by the interconnected network of pores; this one can be increased by a ratio compared to the geometrical distance between the two measured electrodes. Parameters such as the MacMullin number N_M [21–22] and tortuosity τ [23] are used to characterize this behaviour. Both are defined by Eqs. (1) and (2).

$$N_M = \frac{\sigma_0}{\sigma_{eff}} \quad (1)$$

$$\sigma_{eff} = \sigma_0 \frac{\varepsilon}{\tau^2} \quad (2)$$

where σ_0 is the conductivity of pure liquid electrolyte, σ_{eff} is the conductivity of the separator + liquid electrolyte, and ε the porosity ratio.

The MacMullin numbers, N_M, are between 4.7 and 13. N_M numbers are associated with a conductivity decrease related (i) to the porosity structure and (ii) to the affinity between PVdF and the polar electrolyte. The diffusion coefficients of ^{7}Li and ^{19}F were determined by Pulsed Field Gradient spin echo NMR at 30 °C in the liquid electrolyte and in the PVdF separator + liquid electrolyte (Table 4). The experimental conditions are described elsewhere [24]. The diffusion coefficients obtained in the porous membrane are lowered by a factor close to 1.5 than the corresponding diffusion coefficients obtained in the liquid electrolyte, in good agreement therefore with those obtained by Saunier et al. [24]. This mobility decrease was associated with solvent/PVdF interaction; the solvent mobility decrease induces a decrease in ionic species mobility. The cationic transference number t^+, calculated from the diffusion coefficients, $t^+ = \frac{D_{Li}}{D_{Li}+D_F}$, in the macroporous membrane, is equal to that obtained in the liquid electrolyte free of separator, t^+ = 0.4. The invariance in the t^+ value may be associated with the increase in solvent viscosity which affects both anion and cation mobilities. Since the contribution of the swollen inter-pore PVdF to the conductivity of the macroporous membrane is negligible [24], a decrease in the effective electrode surface area may occur. Thus, the lower conductivity value is related to (i) the decrease in diffusion coefficients, (ii) the decrease in effective electrode surface area and (iii) the tortuosity factor.

The best conductivity values, which were obtained with the PVdF-3 and PVdF-4 samples, might be related to their high porous volume.

The highest N_M, i.e. lowest conductivity, was obtained, in accordance with their low porous volume, for PVdF-5 and PVdF-6. A good correlation can be seen between porosity ratio and N_M. Thus the diffusion coefficient decrease may be considered as almost constant for all the samples.

The tortuosity values, determined using Eq. (2), are very close, with a variation between 1.9 and 2.7 for all the samples. Tortuosity allows taking into account the impact of the porous structure and porosity amount on conductivity. Since all the PVdF macroporous samples present near the same poros-

Table 3
Effective conductivity, MacMullin number and tortuosity of LP30® + separator. σ_0 = 9.8 mS cm^{-1} at 21 °C.

Sample	Porosity (%)	σ_{eff} (mS cm^{-1})	N_M	τ	$N_M \times l$
PVdF-1	66 ± 3	1.3 ± 0.1	7.5 ± 0.5	2.2	315 ± 40
PVdF-2	68 ± 2	1.2 ± 0.12	7.7 ± 0.5	2.3	350 ± 44
PVdF-3	77 ± 3	1.9 ± 0.12	5 ± 0.4	2	220 ± 30
PVdF-4	76 ± 3	2.1 ± 0.12	4.7 ± 0.5	1.9	200 ± 30
PVdF-5	58 ± 2	0.9 ± 0.08	10.7 ± 0.5	2.5	750 ± 50
PVdF-6	58 ± 2	0.77 ± 0.08	12.7 ± 0.7	2.7	470 ± 50
PVdF-7	66 ± 3	0.9 ± 0.08	10.8 ± 0.5	2.5	380 ± 40

Table 4
Self-diffusion coefficients of lithium and anion species in macroporous PVdF swelled by liquid electrolyte and in liquid electrolyte.

Sample	D (^{7}Li) (cm^2 s^{-1})	D (^{19}F) (cm^2 s^{-1})
LP30®	2.72×10^{-6}	4.16×10^{-6}
PVdF-3	1.98×10^{-6}	2.76×10^{-6}

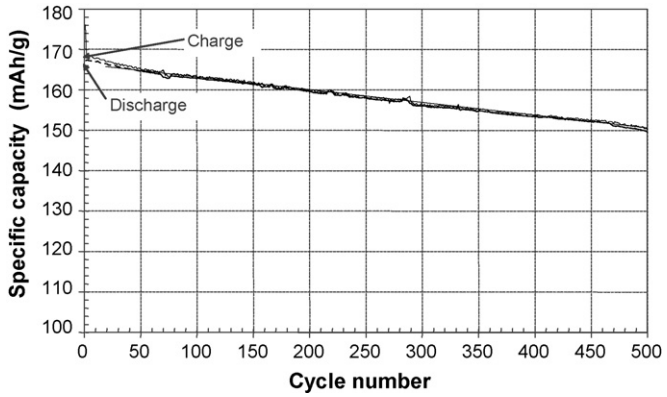

Fig. 3. Changes in charge and discharge capacity during charge–discharge cycles at 25 °C for $Li_4Ti_5O_{12}$/PVdF + liquid electrolyte/$LiMn_2O_4$.

ity structure, a small dispersion in tortuosity values can be obtained.

The MacMullin numbers obtained with PVdF separators are close to the lowest N_M values obtained with Celgard® and Solupor® commercial separators [5]. The good conductivity values obtained with PVdF separators can be associated with their high porosity, large pore diameter and the good wettability of PVdF by carbonate solvents. The calculation of the polymer/solvent interaction, χ_{sp}, defined in the Flory–Huggins theory [25] allows the estimation of the affinity between a polymer and a solvent. The lower the χ_{sp} is, the better the solvent is. Small interaction parameters were found for DMC and EC, $\chi_{sp} = 0.67$ and 0.8 [26] respectively. This clearly indicates a good wettability of the PVdF macroporous membrane by the mixture DMC/EC.

3.3. Battery characterization

The performance of the secondary batteries, $Li_4Ti_5O_{12}$/liquid electrolyte + PVdF separator/$LiMn_2O_4$, was investigated by cycling tests performed at different charge rates. The charge rates used were between *C*/10 and 20*C*. In Fig. 3, changes in charge and discharge capacities at *C*/5 are shown in relation to cycle number. A good cycling ability is obtained, with a reversible capacity of 168 mAh g^{-1} of $Li_4Ti_5O_{12}$ for the first cycle and a loss of 10% of the capacity over 500 cycles. Even at high charge rate, 20*C*, the reversible capacity is high (Fig. 4). The highest capacity obtained at 20*C* charge rate is equal to 103 mAh g^{-1} (average of the first five cycles) with $Li_4Ti_5O_{12}$/liquid electrolyte + PVdF separator/$LiMn_2O_4$ battery.

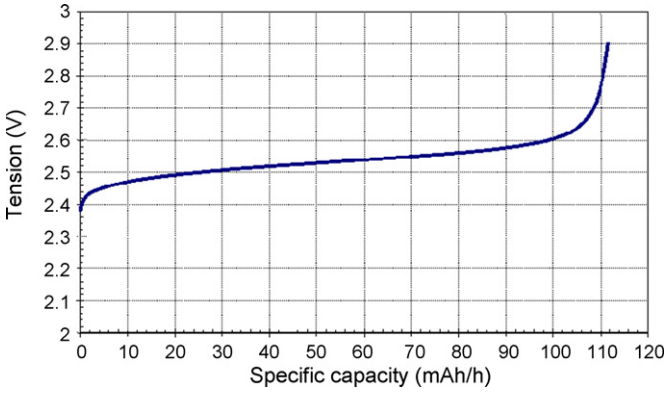

Fig. 4. Specific capacities charged at 20*C* for $Li_4Ti_5O_{12}$/PVdF + liquid electrolyte/$LiMn_2O_4$ (first cycle).

Table 5
Normalized charge capacity for high charge rate, 5*C*, 10*C* and 20*C*. The normalized capacities are expressed as a percentage of the capacity obtained at *C*/10 charge rate. The accuracy of the experiments was determined using the dispersion of the experimental result performed on several cells.

Sample	Porosity (%)	5*C* (%)	10*C* (%)	20*C* (%)
PVdF-1	66 ± 3	93	85	63
PVdF-2	68 ± 2	94	87	65
PVdF-3	77 ± 3	94	86	62
PVdF-4	76 ± 3	95	86	62
PVdF-5	58 ± 2	89	76	48
PVdF-6	58 ± 2	91	78	50
PVdF-7	66 ± 3	94	87	65
Celgard® 2500	53 ± 2	86	77	57
Celgard® 2400	31 ± 4	84	68	38
Solupor® 10P05A	78 ± 2	85	76	54

To better compare the separators, the charging capacities were normalized using those obtained at a low charge rate, *C*/10. The results are presented as a function of charge rate in Table 5.

For charge rates up to 5*C*, the electrochemical performance of the different batteries is roughly similar, in soft cycling condition; the separator morphology has no significant effect on battery performance. Thus the ionic mobility in the electrolyte (liquid + separator) cannot be identified as a limiting process.

At 20*C* charge rate, the batteries with PVdF-5 and PVdF-6 as separators present the lowest capacity with 50% of the capacity obtained at *C*/10 charge rate. These results are in agreement with the N_M numbers. Indeed these two separators present the highest N_M numbers. The batteries using the other samples as separators exhibit almost the same capacity at 20*C* charge rate. The battery with PVdF-7 as a separator exhibits higher cycling performance at 20*C* charge rate than PVdF-5 and PVdF-6 based batteries, despite an N_M number equal to 10.8. This result may be explained by the thickness of the separator, which is thinner than the PVdF-5 separator, which has the same N_M number.

Optimization both of the electrode and the electrolyte is necessary to improve high charge rate performance. For a given liquid electrolyte, the separator + liquid electrolyte can be optimized by minimizing separator thickness and N_M. To characterize this behaviour, Patel et al. [22] recommend using the $N_M \times l$ factor, where l is the thickness of the separator. The lowest capacity values at 20*C* charge rate correspond to the highest $N_M \times l$ factor (Table 5 and Table 3). Thus the $N_M \times l$ factor of the separators seems to be, in our study, a relevant indicator for defining a good separator for use at high charge rates, the number $N_M \times l$ must be lower than 400 μm in our batteries configuration.

For a low $N_M \times l$ value, $N_M \times l < 400$ μm, the $N_M \times l$ factor being irrelevant in the evaluation of the separator electrochemical performance. It might be assumed that, in these batteries, the limitation at high charge rates is not due to the electrolyte but to the electrodes.

The highest capacity obtained at 20*C* charge rate is equal to 103 mAh g^{-1}, thus 13 mAh g^{-1} higher than the best result for commercial polyolefins i.e. 90 mAh g^{-1} with Celgard® 2500, using the same experimental conditions [5]. Furthermore, the lack of capacity at high charge rate is higher with commercial separators i.e. Celgard® 2500, Celgard® 2400, Solupor® 10P05A, than with several PVdF membranes (Table 5).

The ohmic drop, associated with ionic conductivity and thickness, and also the ion concentration gradient might exert an influence on the electrochemical performance of the battery at high charge rates. Indeed, the decrease in ionic mobility induces a decrease in the diffusion coefficient i.e. the Nernst–Einstein relation, and thus an increase in the ion concentration gradient and a decrease in battery performance at high charge rates.

4. Conclusions

PVdF macroporous separators in lithium-ion batteries were investigated during high charge rate cycling tests. The influence of the preparation process on the macroporous PVdF structure was evaluated. The nature of the non-solvent is a parameter that determines the membrane structure. The macroporous PVdF membrane induces a decrease in the conductivity of the liquid electrolyte. Thus, the decrease in conductivity value is related to the decrease in diffusion coefficients and the amount of porosity. The difference in conductivity decrease for the samples tested is largely correlated with the amount of porosity. The PVdf macroporous separator improves the high charge rate performances of $Li_4Ti_5O_{12}$/electrolyte/$LiMn_2O_4$ batteries in comparison with batteries using commercial polyolefin separators.

Acknowledgments

The authors would like to thank the CNRS and the CEA, which awarded a grant to Damien Djian and W. Gorecki for NMR measurements.

References

[1] P.R. Bueno, E.R. Leite, J. Phys. Chem. 107 (2003) 8868–8877.
[2] J. Newman, J. Electrochem. Soc. 1 (1995) 97–101.
[3] S. Atlung, W. West, J. Power Sources 26 (1989) 139–159.
[4] C.R. Sides, C.R. Martin, Adv. Mater. 17 (2005) 125–128.
[5] D. Djian, F. Alloin, S. Martinet, H. Lignier, J.-Y. Sanchez, J. Power Sources 172 (2007) 416–421.
[6] G.B. Appetecchi, F. Croce, A. De Paolis, B. Scrosati, J. Electroanal. Chem. 463 (1999) 248–252.
[7] G.B. Appetecchi, F. Croce, B. Scrosati, Electrochim. Acta 40 (1994) 991.
[8] G. Ardel, D. Golodnitsky, K. Freedman, E. Peled, G.B. Appetecchi, P. Romagnoli, B. Scrosati, J. Power Sources 110 (2002) 152–162.
[9] J.M. Tarascon, T. Gozdz, C. Schmutz, F. Shokoohi, P.C. Warren, Solid State Ionics 86–98 (1996) 49.
[10] A. Du Pasquier, P.C. Warren, D. Culver, A.S. Gozdz, G.G. Amatucci, J.M. Tarascon, Solid State Ionics 135 (2000) 249–257.
[11] D.-J. Lin, C.-L. Chang, C.-L. Chang, T.-C. Chen, L.-P. Cheng, J. Polym. Sci., Part B: Polym. Phys. 42 (2004) 830–842.
[12] A.N. Jansen, A.J. Kahaian, K.D. Kepler, P.A. Nelson, K. Amine, D.W. Dees, D.R. Vissers, M.M. Thackeray, J. Power Sources 81–82 (1999) 902–905.
[13] D. Guyomard, J.-M. Tarascon, J. Electrochem. Soc. 139 (1992) 937–948.
[14] K. Nakahara, R. Nakajima, T. Matsushima, H. Majima, J. Power Sources 117 (2003) 131–136.
[15] A. Bottino, G. Camera-Roda, G. Capannelli, S. Munari, J. Membr. Sci. 57 (1991) 1–20.
[16] J.G. Wijmans, J. Kant, M.H.V. Mulder, C.A. Smolders, Polymer 26 (1985) 1539–1545.
[17] C. Hansen, A. Beerbower, in: A. Standen (Ed.) Kirk-Othmer Encyclopedia Chemical Technology, 2nd ed., Suppl., (1971), 889–910.
[18] (a) F. Boudin, X. Andrieu, C. Jehoulet, I.I. Olsen, J. Power Sources 82 (1999) 804–807;
(b) F. Boudin, PhD thesis, Paris, 1998.
[19] L.-P. Cheng, D.-J. Lin, C.-H. Shih, A.-H. Dwan, C.C. Gryte, J. Polym. Sci. Part B 37 (1999) 2079–2092.
[20] W.D. Wood, J.C. Lacina, B.L. de Prater, J.P. McCullough, J. Phys. Chem. 68 (1964) 579.
[21] K.M. Abraham, Electrochim. Acta 38 (1993) 1233–1248.
[22] K.K. Patel, J.M. Paulsen, J. Desilvestro, J. Power Sources 122 (2003) 144–152.
[23] F.L. Tye, J. Power Sources 9 (1983) 89–100.
[24] J. Saunier, W. Gorecki, F. Alloin, J.-Y. Sanchez, J. Phys. Chem. Part B 109 (2005) 2487–2492.
[25] P.J. Flory, J. Chem. Phys. 10 (1942) 51.
[26] J. Saunier, F. Alloin, J.-Y. Sanchez, B. Barrière, J. Polym. Sci. Part B: Polym. Phys. 42 (2004) 532–543.